International Journal of Engineering Research and General Science Volume 3, Issue 2, March-April, 2015
ISSN 2091-2730

Fault Analysis of Grid Connected Current Source Inverter Based PV System

Saurabh Singh Kashyap, *Student Member, IEEE* and Dr. K.S. Verma, *Professor, K.N.I.T. Sutanpur*

Email:saurabhskashyap@yahoo.com

Abstract- Grid connected or utility interactive PV system are design to operate in parallel with and interconnected with the electric utility grid. The primary component in grid connected PV system is the inverter. The inverter convert DC power produced by the PV array into AC power consistent with voltage, current and power quality requirement of utility grid, and the automatically stops supplying power to the grid when the utility grid is not energized. In voltage source inverter, input voltage is maintained constant and amplitude of output voltage does not depend on the load. However the waveform of load current as well as it's magnitude depends upon the nature of load impedance. In the current source inverter (CSI), input current is constant but adjustable. The amplitude of output current from CSI is independent of load. To enlarge the use of grid-connected PV systems, the cost, performance, and life expectancy of the power electronic interface needs to be improved. The current-source inverter (CSI) offers advantages over VSI in terms of inherent boosting and short circuit protection capabilities, direct output current controllability, and ac-side simpler filter structure. Research on CSI-based DG is still in its infancy. This paper focuses on transient performances of a PV system based on CSI during the rigorous LL and TPG (Three- phase- to-ground) faults. It also performs a comparative analysis of CSI-based PV systems for severe LL and TPG (Three-phase- to- ground) faults under transient conditions. The control structure consists of two current control loops.

An MPPT provides the reference for the outer dc-side current control loop. The inner current control loop is designed to control the current that is injected into the grid. Using a case study of grid-side faults i.e., LL, TPG, the designed controller is able to fulfill all the requirements of a PV system grid interface besides limiting the dc-side current, irrespective of the severity of the fault, unlike a VSI-based PV system. The fault studies included line-to-line and three-phase-to-ground faults. The case study of this paper is presented by using a Mat lab Simulink environment, the respective results also shows the differences between the behavior of a system at the time of encountering faults. To illustrate the Dynamic stability of the CSI-based PV system during transients on the grid side, simulation studies are carried out for four kinds of faults. Results obtained from fault studies are highly in favour of CSI topology and provide illustrative evidence for short-circuit current protection capability of the CSI. On the other hand, the VSI-based PV system performs poorly when subjected to similar grid transients.

I. Introduction

Recently, the inverters are also playing an important role in various renewable energy applications as these are used for grid connection of Wind Energy System or Photovoltaic System. In addition to this, the control strategies used in the inverters are also similar to those in DC-DC converters. Both current-mode control and voltage-mode control are employed in practical applications. The interest in this paper is especially on current source inverters where the load is AC public utility network(through out this paper: the grid), and the source is a PV module. Total PV cell (crystalline silicon PV cell and thin-film PV cell) production in the IEA PVPS countries in 2012 is estimated to be 28,4 GW, about a 5% decrease from the previous year. As in 2011, China reported the largest production of PV cells. Total estimated production of PV cells in China is about 21 GW in 2012. While the growth rate from 2010 to 2011 was about 60%, figure 11 showed only a 5% growth from 2011. 5 companies among China's top 10 producers now have more than 2 GW of manufacturing capacity; Yingli Green Energy with 2,45 GW/year, JA Solar with 2,8 GW/year, Sun tech Power with 2,4 GW/year, and Trina Solar with 2,45 GW/year. Other major IEA PVPS countries producing PV cells are Japan, Malaysia, Germany, the US, and South Korea. In 2012, the IEA PVPS countries accounted for 84% of the global solar cell production. Major non-IEA PVPS countries manufacturing solar cells are Taiwan, Philip-pines, Singapore and India. Major PV module producers in China started to procure solar cells made in Taiwan to avoid the antidumping duties for Chinese solar products in the USA and this brought a growth of solar cell production in Taiwan. 5,4 GW of solar cells were produced in Taiwan in 2012, a 25,6% increase from the previous year.

India is densely populated and has high solar insolation, an ideal combination for using solar power in India. In the solar energy sector, some large projects have been proposed, and a 35,000 km^2 (14,000 sq mi) area of the Thar Desert has been set aside for solar power projects, sufficient to generate 700 to 2,100 GW. Also India's Ministry of New and Renewable Energy has released the JNNSM Phase 2 Draft Policy, by which the Government aims to install 10 GW of Solar Power and of this 10 GW target, 4 GW would fall under the central scheme and the remaining 6 GW under various State specific schemes.

In July 2009, India unveiled a US$19 billion plan to produce 20 GW of solar power by 2020. Under the plan, the use of solar-powered equipment and applications would be made compulsory in all government buildings, as well as hospitals and hotels. On 18 November 2009, it was reported that India was ready to launch its National Solar Mission under the National Action Plan on Climate Change, with plans to generate 1,000 MW of power by 2013. From August 2011 to July 2012, India went from 2.5 MW of grid connected photovoltaic to over 1,000 MW.

Gujarat has been a leader in solar power generation and contributes 2/3rd of the 900 MW of photo voltaics in the country. The State has commissioned Asia's biggest solar park at Charanka village. The park is already generating 2 MW solar power out of its total planned capacity of 500 MW. The park has been functioning on a multi-developers and multi-beneficiaries paradigm and has been awarded for being the most innovative and environment-friendly project by the CII. With a view to make Gandhinagar a solar city, the State government has launched a roof-top solar power generation scheme. Under this scheme, the State plans to generate five megawatt of solar power by putting solar panels on about 50 state government buildings and on 500 private buildings. The State has also a plan to emulate this project in Rajkot, Surat, Bhavnagar and Vadodara in 2012-13.

II. Three-phase Grid-Connected Photovoltaic Module

This paper presents a mathematical modelling for the three-phase grid-connected Photovoltaic (PV) system based on Current Source Inverter (CSI). The paper also discusses designs of controllers for DC-side and AC-side currents. The DC-side current controller is responsible for making the current on the DC side of the inverter track a reference value that corresponds to the maximum power point at a particular insolation level. The AC-side current controller works in coordination with the Coupling (PCC). In this paper, to design current controllers, the phasor quantities are transformed from stationary frame of reference to a rotating frame of reference. Rotating frame of reference reduces number of phasor quantities, thus simplifying the controller design task. A detailed method for transforming the phasor quantities from stationary frame to rotating frame is provided. Model of the CSI developed in this paper is a detailed switched-model simulated in MATLAB simulation package. This paper introduces a simple, yet reliable method to tune the parameters of the controller for independent control of active and reactive components of the current on the AC-side. The single-line diagram of the three-phase, single-stage, grid-connected PV system with a CSI as the power-conditioning unit. The PV array is a parallel combination of np PV modules, while each PV module is a series combination of ns number of PV cells. The DC-side inductor Ldc filters out ripples in the DC-side current and allows its control Figure5.1 illustrates. The AC-side of the inverter is interfaced with the primary side of the transformer Tr through a capacitive filter composed of three Y-connected capacitors, Cf .Function of the capacitive filter, Cf , is to absorb switching harmonics and produce clean sinusoidal current at the grid interface. Breaker Bpv is an integral part of the PV system and is provided to protect the PV system by isolating it when there is a fault on the secondary side of the transformer, Tr.

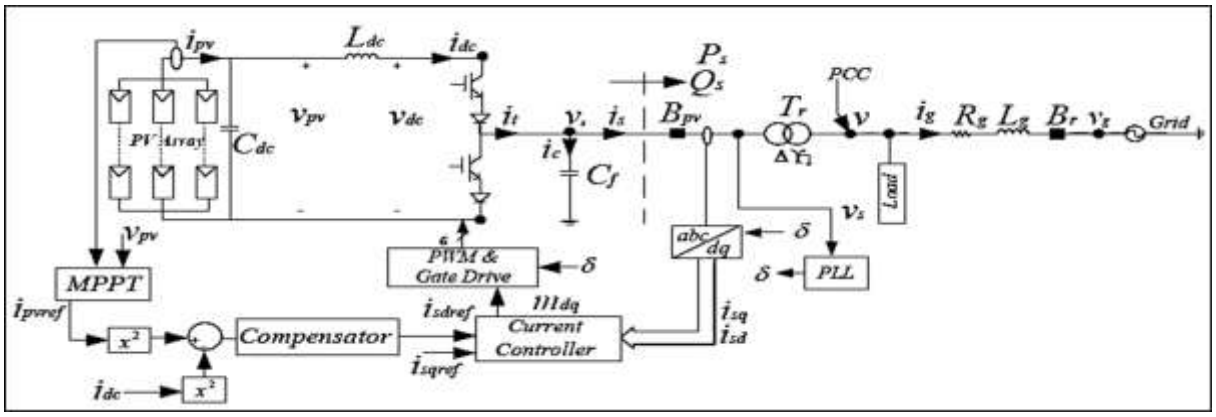

Fig.1: Schematic diagram of a three-phase, single-stage, grid-connected PV system based on CSI.[3]

arrangements for the CSI of Figure 2. Figure 3 illustrates the simulated tri-level terminal current, ita of the CSI. The capacitive filter, Cf suppresses the switching harmonic contents of the terminal current, resulting in the sinusoidal current isa, shown in Figure 3

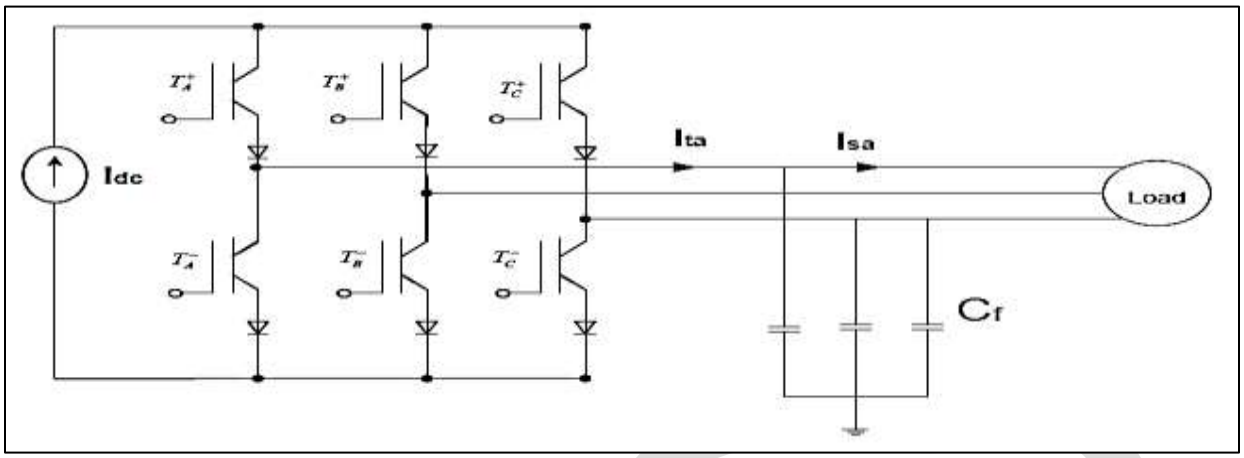

Fig.2 Schematic diagram of a Current Source Inverter.

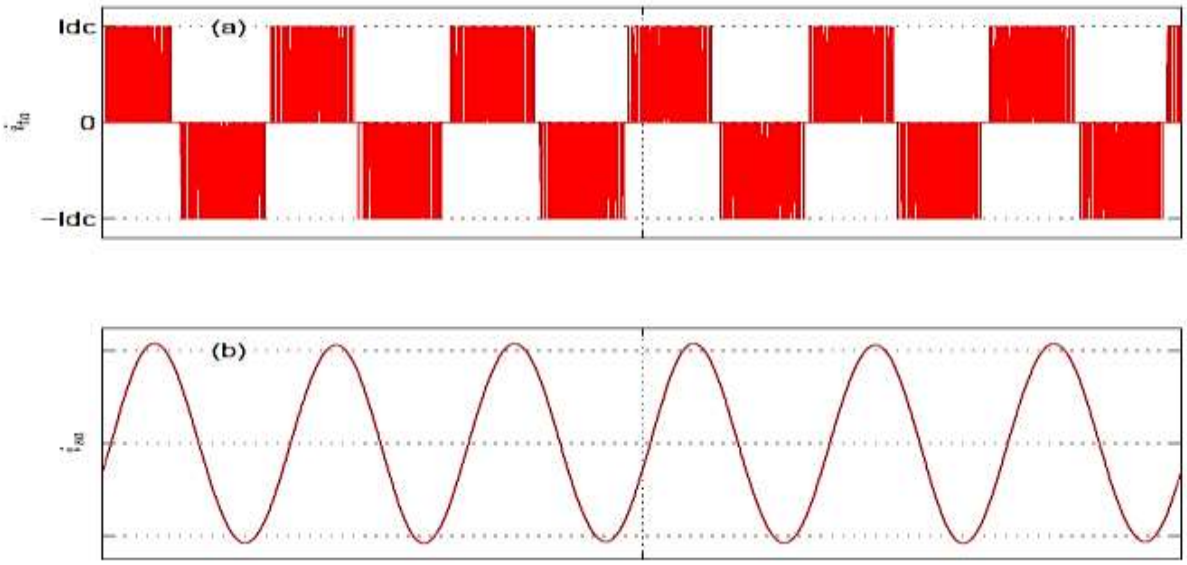

Fig.3: Simulated switching behaviour of the CSI (a) Terminal current of CSI (b) Filtered AC-side current

IV. Dynamics Models of CSI based PV system

A mathematical model is essential for the control design as well as analysis of the PV system. In this section the mathematical model of the uncontrolled PV system is formulated. The overall model consists of three sets of equations which describe the PV matrix, the DC-link voltage dynamics and the AC-side current dynamics of the PV system. The model of the uncontrolled PV system along with those of the controllers constitute a model for the closed-loop PV system.

A. Space-Phasor Representation of the PV System

The PV matrix is described by the following equations [1]:

$$i_{pv} = n_p^i ph - n_p^i rs\ [\exp\left(\frac{q\ u_{pu}}{kT_c\ n_x}\right) - 1] \quad (1)$$

where *q* is the unit charge, *k* is Boltzmann's constant, *A* is the p-n junction ideality factor, and *Tc* is the cell temperature. *Irs* is the cell reverse saturation current, which varies with temperature according to the following equation:

$$i_{rs} = i_{rr}[\frac{T_c}{T_r}]^3 \exp\left(\frac{qE_G}{kA}\left[\frac{1}{T_r} - \frac{1}{T_e}\right]\right) \quad (2)$$

where *Tr* is the cell reference temperature, *Irr* is the reverse saturation current at *Tr*, and *EG* is the band-gap energy of the cell. The photovoltaic current, *Iph*, depends on the insolation level and the cell temperature as:

$$i_{ph} = [i_{scr} + K_e(T_c - T_r)]\frac{S}{S_{STC}} \quad (3)$$

In (2), iscr is the cell short-circuit current in Amperes at the reference temperature and irradiation, K a temperature coefficient, S the insolation in kW=m2 and SSTC the insolation level at standard temperature condition (STC) which is equal to 1 kW=m2.Power delivered by the PV array is calculated by multiplying both sides of (3) by vpv.

$$P_{pv} = n_p i_{ph} u_{pv} - n_p i_{rs} u_{pv}\left[\exp\left(\frac{q\,u_{pv}}{kT_c A n_s}\right) - 1\right] \quad (4)$$

Substituting current iph from (3) in (4), power Ppv becomes

$$P_{pv} = n_p[i_{scr} + K_\theta(T_c - T_r)]\frac{S}{S_{STC}}u_{pv} - n_p i_{rs} u_{pv}\left[\exp\left(\frac{q\,u_{pv}}{kT_c A n_s}\right) - 1\right] \quad (5)$$

Based on (5), [3] it is evident that the power delivered by the PV array is a function of insolation level, S, at any given temperature. Since the inverter employed in the PV system of this work is of current-source type. The power-versus-current characteristic of the PV array has to be examined (rather than the power-versus-voltage characteristic). Figure 4 illustrates the power-versus-current characteristic of the PV array based on the parameters listed in the Appendix A for insolation levels of 0.1, 0.5 and 1 kW=m2. Figure 5.4 shows that Ppv can be maximized by control of current ipv, based on a Maximum PowerPoint Tracking (MPPT) strategy [7].

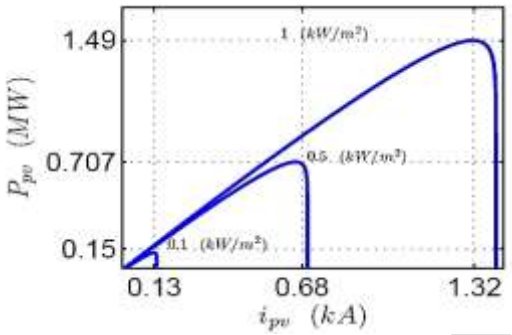

Fig.4:Current versus power characteristics of a PV matrix

The output current of the CSI, i_t is related to the DC-side current idc as follows [3]

$$\vec{i_t} = \vec{m} i_{dc} \quad (6)$$

Where $\dot{t}$ and $\dot{m}$ are the space phasors corresponding to the CSI terminal currents and the PWM modulating signals. The CSI of Figure 2 is a 6-pulse converter employing IGBT switches, operated under Sinusoidal Pulse Width Modulation (SPWM) strategy [2]. Similarly, the DC-side voltage, vdc, is related to the CSI AC-side voltage space phasor as [3]

$$u_{dc} = \vec{m} v_s \quad (7)$$

Voltage and current at the PCC can be expressed in space-phasor form as [1]:

$$\vec{u_s} = \frac{2}{3}\left(v_{sa} + e^{-j\frac{2\pi}{3}}u_{sb} + e^{j\frac{2\pi}{3}}u_{sc}\right) \quad (8)$$

And

$$\vec{i_s} = \frac{2}{3}\left(i_{sa} + e^{-j\frac{2\pi}{3}}i_{sb} + e^{j\frac{2\pi}{3}}i_{sc}\right) \quad (9)$$

$$\vec{i_s} = \frac{2}{3}\left(i_{sa} + e^{j\frac{2\pi}{3}}i_{sb} + e^{-j\frac{2\pi}{3}}i_{sc}\right) \quad (10)$$

Multiplying (8) and (9), and considering real parts of both sides one gets

$$Re\{\vec{u_s}\vec{i_s}\} = \frac{4}{9}(u_{sa}i_{sa} + u_{sb}i_{sb} + u_{sc}i_{sc}) - \frac{u_{sa}i_{sb}}{2} - \frac{u_{sa}i_{sc}}{2} - \frac{u_{sb}i_{sa}}{2} - \frac{u_{sb}i_{sc}}{2} - \frac{u_{sc}i_{sa}}{2} - \frac{u_{sc}i_{sc}}{2} \quad (11)$$

Equation (11) can be further simplified to

$$Re\{\vec{v_s}\vec{i_s}\} = \left[\frac{4}{9}(u_{sa}i_{sa} + u_{sb}i_{sb} + u_{sc}i_{sc}) - \frac{1}{2}(u_{sa} + u_{sb} + u_{sc})(i_{sa} + i_{sb} + i_{sc})\right] \quad (12)$$

For a balanced three-phase system currents, isa, isb, isc are related as:

$$i_{sa} + i_{sb} + i_{sa} = 0 \quad (13)$$

Substituting (13) in (12) one gets

$$Re\{\overrightarrow{u_s}\,\overrightarrow{i_s}\} = \frac{2}{3}(v_{sa}i_{sa} + u_{sb}i_{sb} + u_{sc}i_{sc})$$

For a three-phase systems the real power, Ps in time domain is expressed as [1]:

$$P_s = (u_{sa}i_{sa} + u_{sb}i_{sb} + u_{sc}i_{sc})$$

Substituting expression for Ps from (12) in (13) one gets

$$Re\{\overrightarrow{v_s}\,\overrightarrow{i_s}\} = \frac{2}{3}P_s \quad (14)$$

Equation (14) can be rewritten as

$$P_{dc} \approx P_s = \frac{3}{2}Re\{\overrightarrow{v_s}\,\overrightarrow{i_s}\}$$

Assuming the switching losses of the inverter negligible, the DC-side power of the inverter, Pdc, is equal to the power delivered on the AC-side. Therefore [3],

$$P_{dc} \approx P_s = \frac{3}{2}Re\{\overrightarrow{v_s}\,\overrightarrow{i_s}\} \quad (15)$$

B. DQ-Frame Representation

For the purposes of analysis and control, the space-phasor variables of the PV system model are projected on a *dq*-frame. Transformation of the variables from the space-phasor form to the *dq*-frame form results in equivalent DC variables, which simplify the analysis and control design tasks. Moreover, a *dq*-frame based control can be implemented more conveniently compared to the case where the control signals are time-varying. The transformation is defined as:

$$\vec{f} = (f_d + jf_q)e^{jp} \quad (16)$$

Where $\vec{f}$ represents a space-phasor, *fd* and *fq* are the space-phasor *dq*-frame components,
and ρ is the reference angle of the *dq*-frame. Another useful quantity isthe derivative of a space-phasor, that is:

$$\frac{d\vec{f}}{dt} = \frac{d\left|(f_d + jf_a)^{e^{jp}}\right|}{dt}$$
$$= \left(\frac{df_d}{dt} + \frac{df_q}{dt}\right)e^{jp} + j\frac{d_q}{dt}(f_d + if_q)d^{jp}$$
$$= \left(\frac{df_d}{dt} + \frac{df_q}{dt}\right)e^{jp} + j\omega(f_d + jf_a)d^{jp}$$

where ω is the *dq*-frame angular speed, as

$$\omega = \frac{dp}{dt}$$

Based on (16), *Ps* in (13) can be expressed as:

$$P_s = \frac{3}{2}Re\left\{\frac{(v_{sd}+jv_{sq})d^{jp}}{\vec{v}_s}\frac{(i_d+ji_q)d^{-jp*}}{\overrightarrow{r^2}}\right\} \quad (17)$$

which can further be simplified to

$$P_s = \frac{3}{2}(v_{sd}i_d + v_{sq}i_q) \quad (18)$$

Similarly, the *dq*-frame equivalent of *PR* in (18) is deduced as:

$$P_R = \frac{3}{2} R \left(i_d^2 + i_q^2\right) \quad (19)$$

In addition, based on (18) and (19), *PL* in (19) is simplified to

$$P_L = \frac{3}{2} L \left(i_d \frac{d_{id}}{dt} + i_q \frac{di_q}{dt}\right) \quad (20)$$

Substituting in (20) for *Ps*, *PR*, and *PL*, respectively from (17), (18), and (19) one finds:

$$\frac{C}{2} \frac{dv_{dc}^2}{dt} = P_{Pv} - \frac{3}{2} \left(v_{sd} id + v_{sq} i_q\right) - \frac{3}{2} R \left(i_d^2 + i_q^2\right) - \frac{3}{2} L \left(i_d \frac{d_{id}}{dt} + i_d \frac{d_{iq}}{dt}\right) \quad (21)$$

Equation (21) is employed in designing a voltage regulator to maintain the DC link voltage, *vdc*, at a desired level, such that the power out of the PV matrix can be maximized. A similar procedure as the one adopted to derive (22) yields the following *dq*-frame equivalents for (20):

$$L \frac{d_{id}}{dt} = L\omega i_q - R_{id} + m_d \frac{v_{dc}}{2} - v_{sd} \quad (22)$$

$$L \frac{d_{iq}}{dt} = -L\omega i_q - R_{iq} + m_d \frac{v_{dc}}{2} - v_{sq} \quad (23)$$

Equations (21), (22), and (23) constitute a state-space model for the VSC, in which v^2dc, *id*, *iq* are the state variables, *md* and *mq* are the control inputs, and *vsd*, *vsq*, and *S* are the exogenous inputs.

C. Phase-Locked Loop (PLL)

As discussed in previous Section, the AC variables of the PV system are projected on a *dq* frame the rotational speed of which is ω In a steady state, the AC variables are sinusoidal functions of the grid frequency ω_0. Thus, their *dq*-frame components become time-invariant (in the steady-state) if the *dq* frame angular speed ω becomes equal to ω_0. This is achieved by means of a PLL mechanism [5]. A block diagram of the PLL adopted in this research is presented in Figure. 5. As Figure.5 shows, $\widetilde{vs}$is resolved into its *d* and *q* axis components, based on (20). Then, *vsq* is processed by the compensator *H*(*s*), and ω is determined. In a steady state, *vsq* is forced to zero while ω becomes equal to ω_0. Therefore, *H*(*s*) must include at least one integrator.

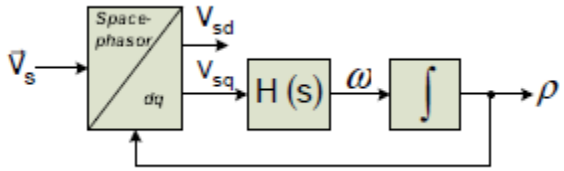

Fig.5: Block diagram of the Phase-Locked Loop (PLL)

Let *H*(*s*) be a PI compensator cascaded with a first-order, low-pass, transfer function, as

$$\Omega = H(s) V_{sq}$$

$$= \frac{\beta_1 s + \beta_2}{s(s + \beta_3)} V_{sq}$$

where $\beta 1$ and $\beta 2$ are the proportional and integral gains of the PI part, respectively,whereas β3 is the pole of the low-pass function of the compensator. Let the two state variables β1 and β2 are defined as

$$x_7 = \frac{v_{sq}}{s^2 + \beta^{3s}}$$

$$x_6 = sX_2$$

then, the PLL is described by the state-space model

$$\frac{d}{dt}x_{pll} = A_{pll}X_{pll} + B_{pll}\begin{vmatrix} v_{sd} \\ v_{sq} \end{vmatrix}$$

$$\omega = E_{pll}X_{pll}$$

$$\rho = F_{pll}X_{pll}$$

Where

Where $A_{pll} = \begin{vmatrix} -\beta_2 & 0 & 0 \\ 1 & 0 & 0 \\ \beta_1 & \beta_2 & 0 \end{vmatrix}$

$$B_{pll} = \begin{vmatrix} 0 & 1 \\ 0 & 0 \\ 0 & 0 \end{vmatrix}$$

$$E_{pll} = |\beta_1 \beta_2\ 0|$$

$$F_{pll} = |0\ 0\ 1|$$

$$X_{pll} = |x_6\ x_7\ \rho|^T$$

Equations introduce the PLL as a dynamic system whose inputs are *vsd* and *vsq*, the state variables are ε1, ε2, and ρ and the outputs are ρ and ω. Regulation of *vsq* at zero also has the implication that the expression for the PV system real-power output, i.e. (5.24), is simplified to

$$P_s = \frac{3}{2}\, v_{sd} i_d \qquad (24)$$

Hence, *Ps* is proportional to, and can be controlled by, *id*. Similarly, the *dq*-frame expression for the reactive power assumes the form:

$$Q_s = \frac{3}{2} Im\{\overrightarrow{u_s}\ \overrightarrow{i_s}\}$$
$$= \frac{3}{2} v_{sd} i_{sq} \left\{ \frac{[(u_{sd} + ju_{sq})e^{jb}]}{j_b}\ \frac{[(i_{sd} + ji_{sq})e^{jb}]}{j_b} \right\}$$
$$= -\frac{3}{2}\, u_{sd} i_{sq}$$

which can be further simplified to:

$$Q_s = -\frac{3}{2} v_{sd} i_q \qquad (25)$$

Equation (25) indicates that *Qs* can be controlled by *iq* to adjust the power-factor that the PV system exhibits to the distribution network.

V. Inner Current Control Loop

Equations (24) and (25), respectively, show that active and reactive powers delivered by the CSI can be adjusted by controlling isd and isq, respectively. Figure 6 shows the

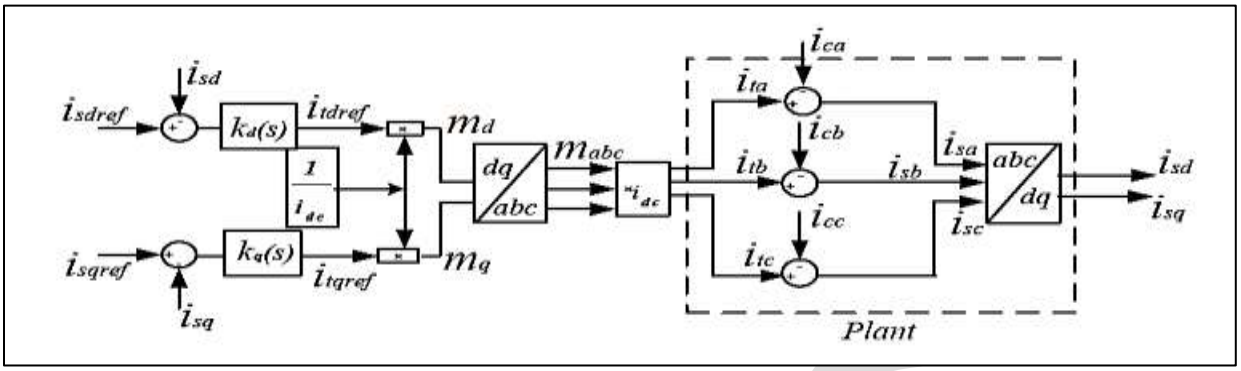

Fig.6: Block diagram of the CSI AC-side current control system [3]

block diagram of the CSI AC-side current controller. Controller structures kd(s) and kq(s) in Figure 5.6 are expressed as:

$$k_d(s)=k_q(s)=k_p+\frac{k_i}{s} \quad (26)$$

where kp nd ki are the proportional and integral gains, respectively. Control signals md and mq are obtained as

$$m_d=\frac{i_{tdref}}{i_{dc}} \text{ and } m_q=\frac{i_{tqref}}{i_{dc}} \quad (27)$$

where i_{tdref} and i_{tqref} are current references derived from the outputs of the compensators kd(s) and kq(s), respectively. The d-axis component of the inverter output current, itd, is related to the current isd as:

$$i_{td}=i_{cd} \quad (28)$$

where icd is d-axis component of the filter capacitor current. It should be noted that with a proper filter design, the fundamental-frequency component of the capacitor current will be very small, i.e., icd is negligible as compared to isd. The same discussion can be made for the q-axis components. Therefore, one can write

$$i_{td}\approx i_{sd}\approx m_d i_{dc} \text{ and } i_{tq}\approx i_{sq}\approx m_q i_{dc} \quad (29)$$

Under the assumption that icd =0, the following transfer function can be written for the closed-loop control system of isd illustrated in Figure 6.

$$T(s)=\frac{i_{sd}}{i_{sdref}}=\frac{k_p+\frac{K_i}{s}}{s+\frac{1}{T_i}}=\frac{s\frac{k_p}{k_p+1}+\frac{k_i}{k_p+1}}{s+\frac{k_i}{k_p+1}} \quad (30)$$

As the value of kp increases the pole of the transfer function T(s) in (30) approaches the origin of s-plane, which is not desirable. Therefore, to imitate the transient behaviour of a first-order system, kp should be chosen to be small. ki, as the inverse of time-constant. Thus, kp and ki can be written as:

$$k_p\approx 0 \text{ and } k_i=\frac{1}{T_i} \quad (31)$$

Substituting the values of kp and ki in (31) the transfer function T(s) becomes

$$T(s)=\frac{i_{sd}}{i_{sdref}}=\frac{\frac{1}{T_i}}{s+\frac{1}{T_i}}=\frac{1}{T_i s+1} \quad (32)$$

In the first order system represented by (32), i determines the controller response time. For fast response, the range of i varies between 0.5 ms to 5 ms.

VI. Outer Current Control Loop

Equation (26), after substituting vsq = 0, represents a system with isd as the input, i^2dcthe output and vsd the disturbance input. If time constant τ in the PI compensator of the inner current control loop is properly selected, isd can be approximated to isd(ref) Therefore,(26) can be rewritten as:

$$\frac{1}{2}L_{dc}\frac{di_{dc}^2}{dt} \approx P_{pv} - \frac{3}{2}u_{sd}i_{sdref} \quad (33)$$

The DC-link current controller designed on the basis of (33) is illustrated in Figure7. The fact that Ppv is product of vpv and ipv makes the system nonlinear. To mitigate the impact of nonlinearity, isdref can be derived in the following way:

$$i_{sdref} = u_i + n\left(\frac{P_{pv}}{\frac{3}{2}u_{sd}}\right) \quad (34)$$

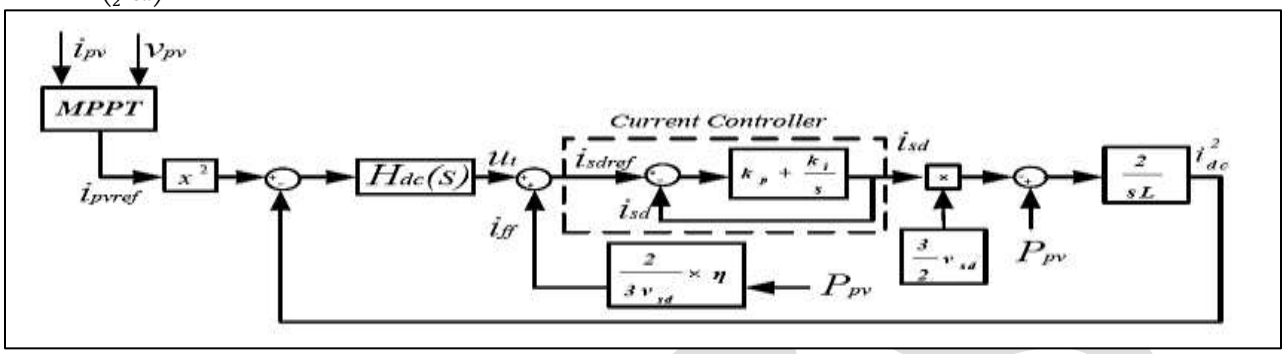

Fig.7: Closed-loop control structure of the DC-side current [3]

$$\frac{L_{dc}}{2}\frac{di_{dc}^2}{dt} \approx (1-\eta\ )p_{pv} - \frac{3}{2}u_{sdu_i.} \quad (35)$$

Equation (35) indicates that if η = 1, the impact of the PV array nonlinearity on the DC side current control is eliminated, and the effective control unit becomes an integrator.

VII. Comparative Performance of the CSI-based PV system with the VSI based PV system

Case study 1: On Different Insolation Level of PV Panels

In this case study, the behaviors of the VSI- and CSI-based PV systems in response to a change in insolation level are illustrated. Since VSI and CSI are dual topologies, the characteristic of voltage in CSI is analogous to that of current in VSI, and vice versa. Initially, the insolation level is set to 0.4 kW=m2. At t = 1 s, the insolation level is step changed to 0.6 kW=m2, as shown in Figure 8.1(a). With the change in insolation level, the CSI DC-side current reference changes from 0.7 kA to 1 kA by the maximum power point tracker. The new reference is tracked by the outer current control loop or the DC-side current controller, as shown in Figure 8.1(c). Since the terminal current of the CSI, it, is linearly related to the DC-side current, idc, it is also changed as shown in Figure 8.1(e). The AC-side current reference is derived from the DC-side current control loop. Since there is an increase in the DC-side current, the d-axis current reference, i_{tdref}, increases, and so does the current isa, as shown in Figure 8.1(g). With the increase in isa, the current on the secondary side of the transformer, iga, also increases. Presently, the utility mandates that the current injected by the inverter, iga, be in-phase with the voltage at the PCC. This is shown in Figure 8.1(b). Figures 8.1(b),(d),(f) show the performance of a VSI-based PV system in response to the same step change in insolation level. One can observe in Figure 8.1(d) a step change in the DC-side voltage level, vdc, of the VSI as a result of a change in insolation level, similar to that in DC-side current of CSI. The AC-side terminal voltage of VSI, shown in Figure 8.1(j), is a two-level quantity whereas the AC-side terminal current of CSI is a three-level quantity. Figure 8.1(h) illustrates the filtered output voltage of the VSI. The unity power factor maintained by the VSI-based PV system at the PCC is illustrated in Figure 8.1(i). From this case study, it can be inferred that the performance of the CSI-based PV system is quite satisfactory and even superior to that of VSI-based PV system due to three-level output current (as compared to two-level output voltage of (VSI), simpler AC-side filter design and direct control of injected current (as compared to indirect output current control in VSI).

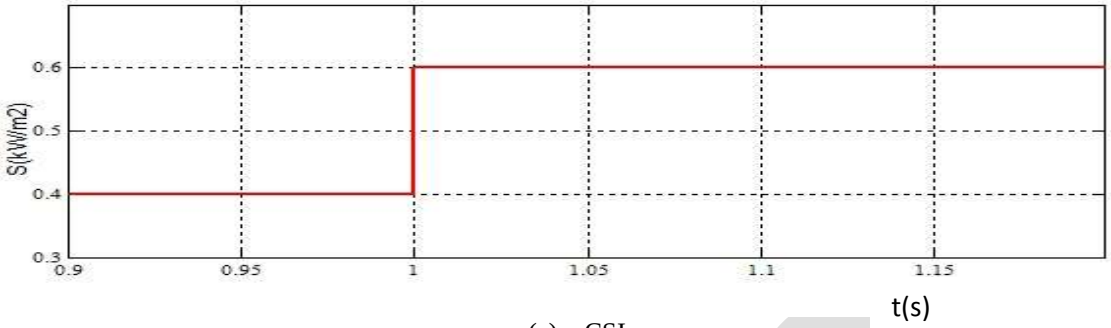

(a) CSI

(b) VSI

Fig. 8.1: (a) and (b) S =Insolation level

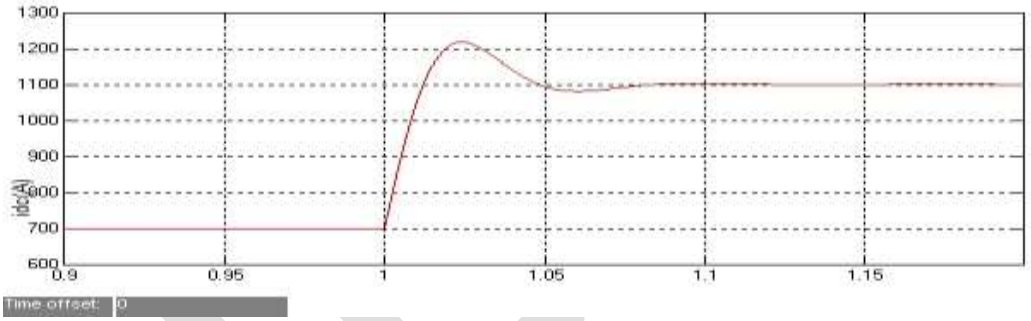

(c) CSI

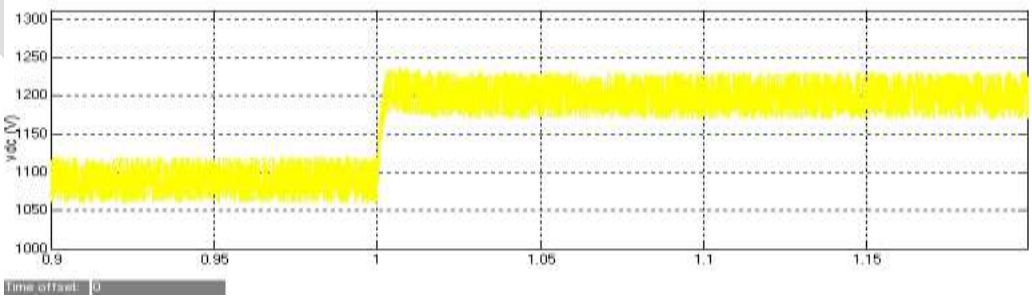

(d) VSI

Fig.8.1: (c) and (d) idc = DC-side current of CSI; vdc = DC side voltage of VSI

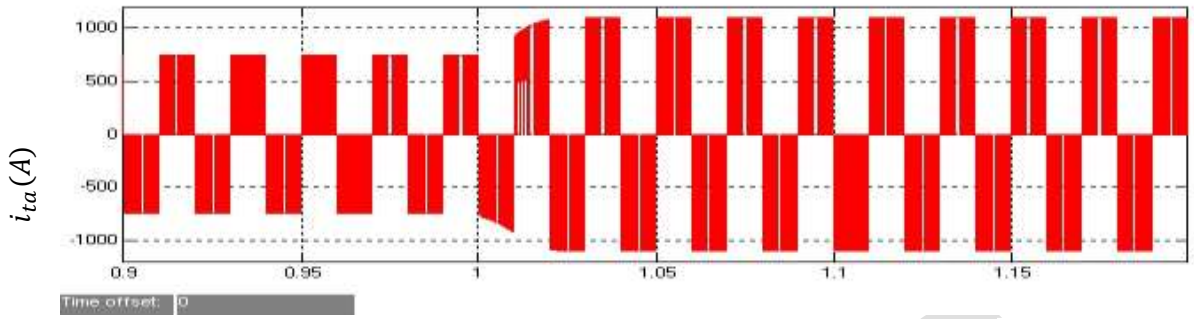

(e) CSI

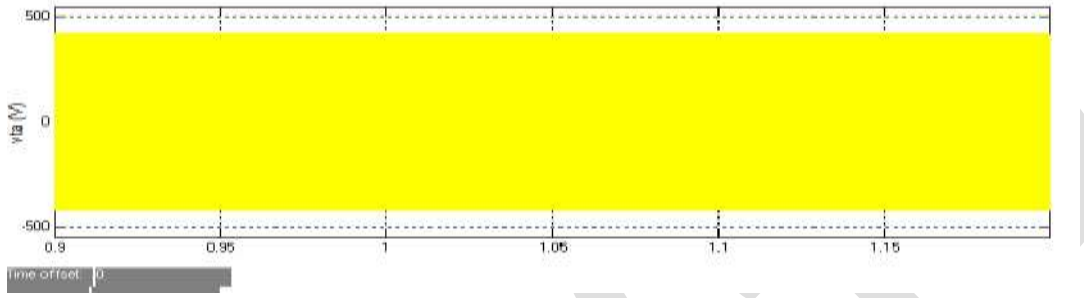

(f) VSI

Fig.8.1: (e) and (f) ita = Phase-a AC terminal current of CSI; vta = Phase-a AC terminal voltage of VSI

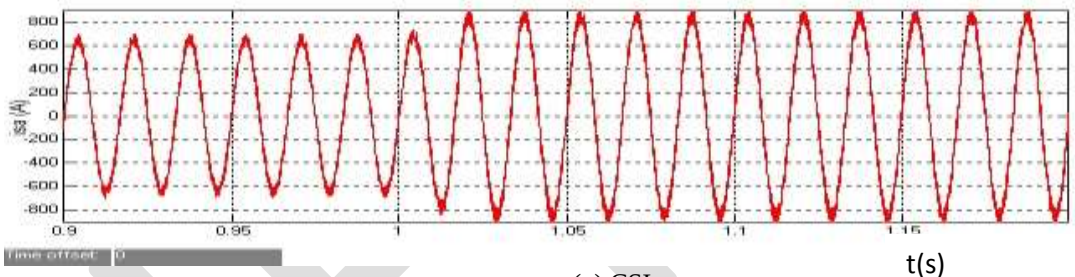

(g) CSI

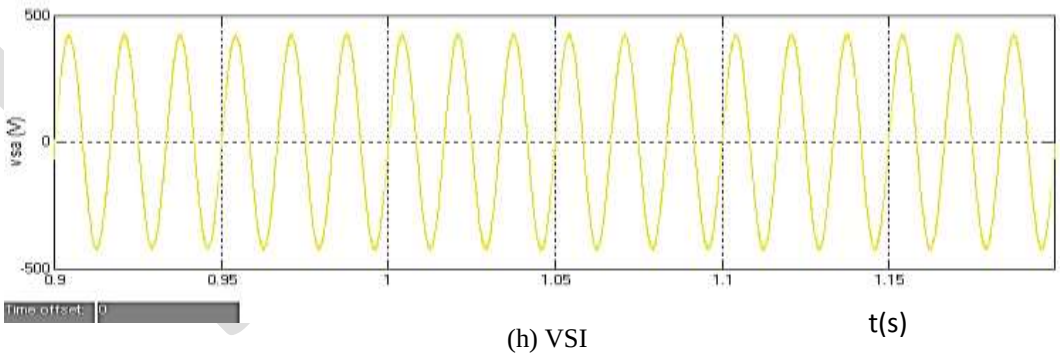

(h) VSI

Fig.8.1: (g) and (h) isa CSI phase-a filtered current injected into the grid; vsa = VSI phase-a filtered voltage at the grid interface

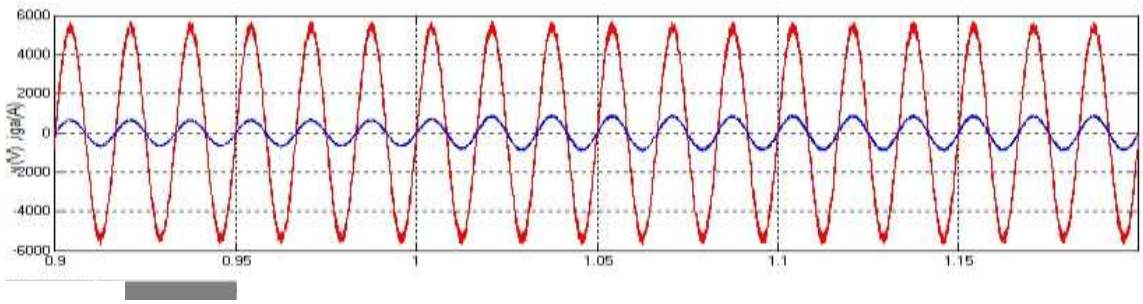

(i) CSI

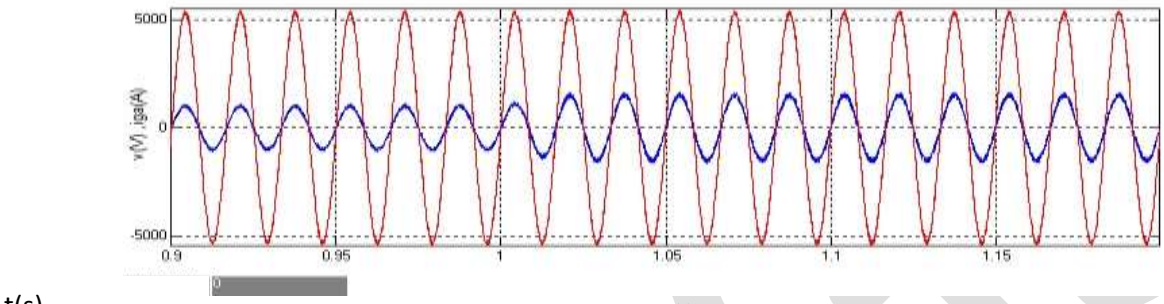

(j) VSI

Fig.8.1: (i) and (j) v = Phase-a voltage at the PCC; iga = Phase-a current at the PCC

Case study 2: When Fault Occurs

The objective of this case study is to show the impact of a change in the AC-side voltage level on the performance of the PV system, the anti-islanding protection is disabled. At time t = 1.5 s, a SLG fault is applied on phase-a of secondary side of the transformer Tr. Due to the fault, the voltage va drops to zero, as shown in Figure 8.2(a). Application of fault on the AC-side has resulted in oscillations in the DC-side current of the CSI, as shown in Fig. 8.2(b). However, oscillations are damped as soon as the fault is cleared, and the DC-side current controller tracks the reference current in less than 20 ms. Due to this disturbance, the AC terminal current of the CSI, ita, undergoes over modulation, as shown in Figure 8.2(c). The over modulation results in low order harmonics, and the current isa injected into the grid is no longer sinusoidal, as shown in Figure 8.2(d). This case study clearly shows the inherent over-current protection built in CSI that limits the currents on both DC and AC sides. Fault on the grid-side of the inverter results in oscillations of current and voltage on the DC-side of the inverter [4], [5] Oscillations in the DC-side current are not desirable as the inverter requires a smooth input DC-current. In case of VSI-based PV system, the controller regulates the DC-side voltage; therefore, there is no direct control on the DC side current. On the contrary, in CSI-based PV system, the DC-side current is regulated and limited. As a result, the current on the AC-side of the inverter may not show a sharp rise under fault. This case study is designed to present a comparative analysis of behaviors during fault for CSI- and VSI-based PV systems. For this study, the insolation level is maintained at 1 kW=m2. In real life, when the fault occurs on the grid-side, and the breaker Br opens, the anti-islanding scheme must act to protect the inverter and personnel.

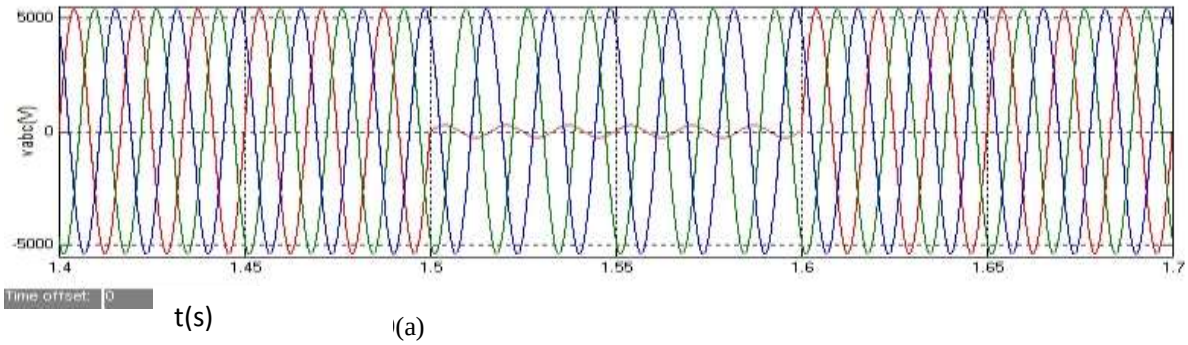

(a)

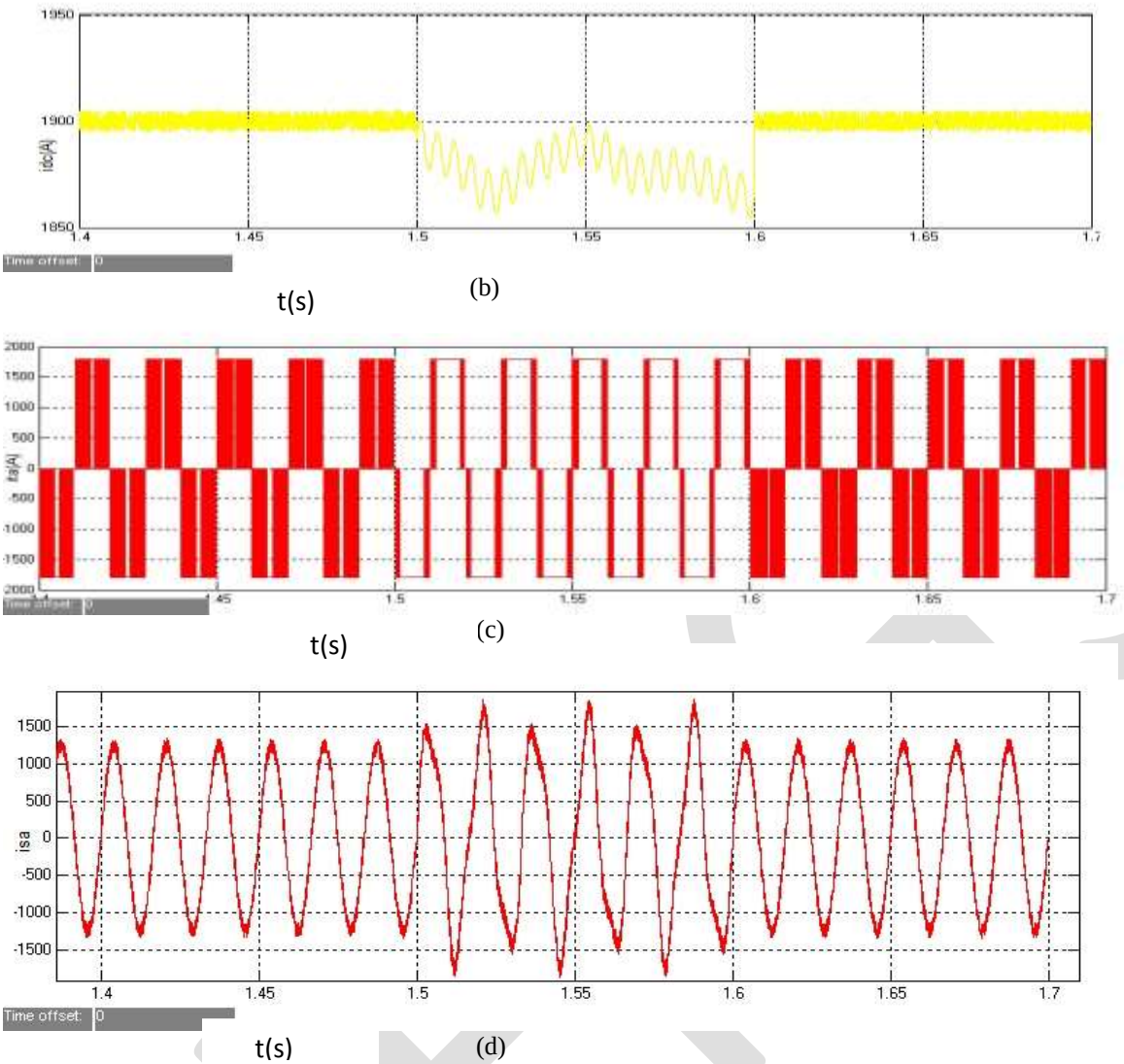

Fig. 8.2: CSI-based PV system performance during SLG (vabc = three phase voltage on the secondary-side of Tr; idc = DC-side current of the CSI; ita = phase-terminal current of CSI; isa = phase-a current injected to the grid).

VIII. CSI and VSI Relative Performances During Single line to Ground Fault

The performances of CSI- and VSI-based PV systems during a SLG fault. As mentioned earlier, in VSI-based PV system, the controller on the DC-side is employed to control the DC-side voltage (with AC-side currents limited during faults by limiters implemented in the control system), whereas in CSI-based PV system, the controller's task is to control the DC-side current. One can observe from Figure 9(a) that the range of variation in the DC-side current of CSI during fault is tightly limited due to the regulatory role of the DC-side current controller. On the contrary, Figure 9(c) shows that the DC-side current of VSI is allowed to vary in a wide range. Also, Figure 9(b) shows that the amplitude of CSI's AC-side current is limited during fault, whereas the AC-side current of VSI shows a sharp rise in the presence of a current limiter, as illustrated by Figure 9(d).

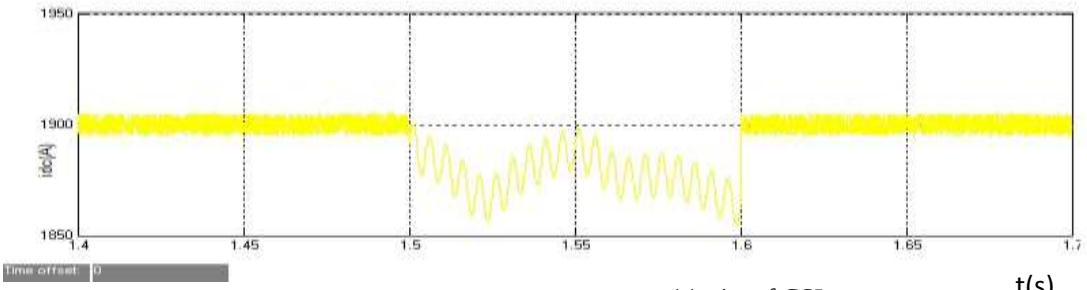

(a) i_{dc} of CSI

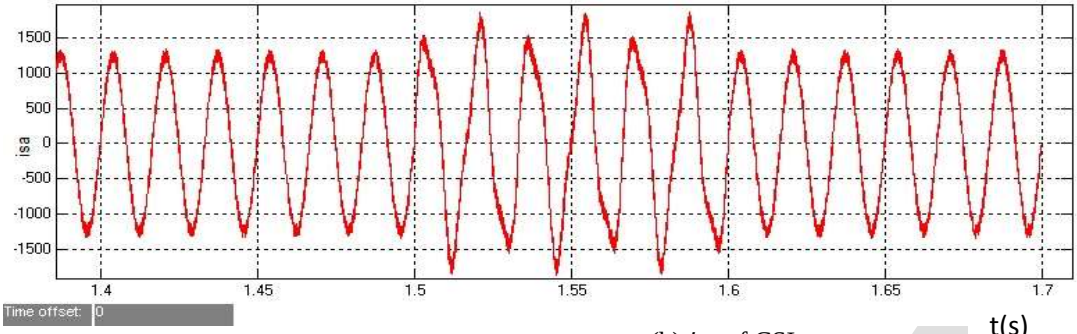

(b) i_{sa} of CSI

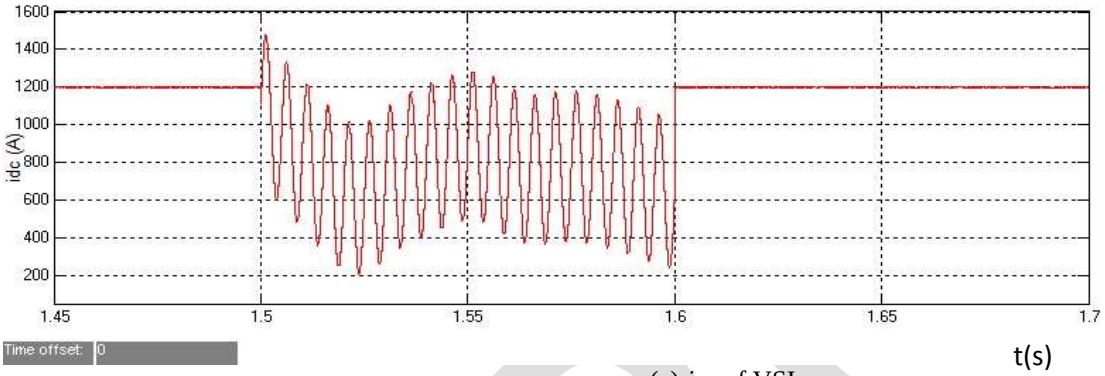

(c) i_{dc} of VSI

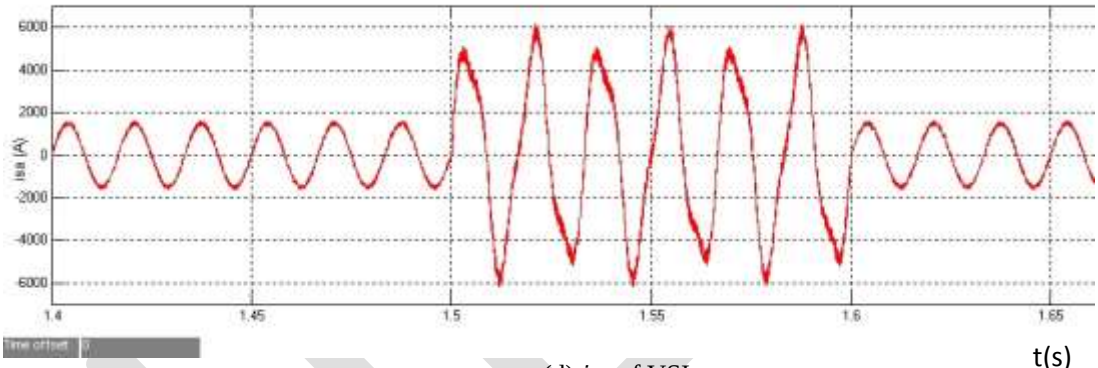

(d) i_{sa} of VSI

Fig.9: CSI- and VSI-based PV systems' performances during a SLG fault.

Conclusion

The main objective of this paper is to make quality contributions in the field of power electronic interface for grid-connected PV systems. For this purpose, the less-investigated topology for PV system grid interface, i.e., Current Source Inverter was chosen. To make sure about the originality of the work and to avoid repetition of the past work, an extensive literature survey was carried out first. The literature survey covers a range of topologies employed for interfacing PVs. A part of literature survey focusses on grid-connected PV systems that incorporate CSI as their power conditioning units. The survey was a useful way to determine the research gap in the field of CSIs for PV applications. In the initial stage of research, a single-stage CSI-based PV system was designed. The design involved developing a DC-link current controller, which allowed maximum power point tracking, and an AC-side current controller with the mandates of AC-side current wave shaping and reactive power control. The maximum power point tracker (MPPT) is based on the widely used Perturb & Observe (P&O) method and can track the maximum power point in the order of milliseconds. To efficiently track the current reference generated by the MPPT, DC-link current controller is equipped with a feed-forward compensation technique. The feed-forward control plays a major role in suppressing the nonlinearity caused by PV arrays.. The AC-side current controller is designed in a stationary frame of reference. For converting the 3-phase state variables to their corresponding dq-frame equivalents, the transformation angle is derived from the Phase-Locked Loop (PLL). The task of the AC-side current

controller is to track the reference for the d-axis component of AC-side current, generated by DC-link current controller, and inject a clean sinusoidal current into the grid that is in phase with the voltage at the PCC. The AC-side current controller has the exibility of adjusting reactive power to a desired value. However, for this work, it is assumed that there is no reactive power demand from the PV system. Therefore, the reactive component is set to zero and there is only active power transfer between the PV system and the distribution system. To verify the performance of the developed CSI-based PV system, a number of simulation studies are carried out in Matlab environment. In the first case study, the performance of the CSI-based PV system is compared with that of a VSI-based PV system of similar rating for a step change in the insolation level. Through simulation results, it is shown that even though both topologies show similar performances, the quality of the sinusoidal current generated by a CSI-based PV system is superior to that of the current generated by a VSI-based PV system. To illustrate the performance of the CSI-based PV system during transients on the grid side, simulation studies are carried out for four kinds of faults. Results obtained from fault studies are highly in favor of CSI topology and provide illustrative evidence for short-circuit current protection capability of the CSI.

SYSTEM PARAMETERS

PV system parameter	**Value**	**Comment**
filter capacitance, Cf	300 uF	
switching frequency	3060 Hz	51× 60 Hz
DC-link capacitance, C	1000 uF	
DC-link inductance, Ldc	1 mH	
ns of PV cells per string, ns	800	
np of PV strings, np	200	
ideality factor, A	1.92	
cell reference temperature, Tref	300 K	
temperature coefficient, kV	0.0017 A/K	
cell short circuit current, Iscr	8.03 A	
reverse saturation current, Irs	1.2 10^{-7} A	
Grid inductance, Lg	1 mH	
Grid Resistance, Rg	1 m	
Grid voltage, vg	6.6 kV	
Tr nominal power	1.3 MV A	
Tr voltage ratio	6.6/0.48 kV	Delta/Y
Tr leakage inductance	0.1 pu	
Tr ohmic resistance	0.02 pu	
on-state resistance of valves, R	3 m	
kp (for i = 0.5 ms)	.0002	
ki (for i = 0.5 ms)	2 s-1	

REFERENCES:

[1] R. Singh, G. F. Alapatt, and K. F. Poole, "Photovoltaics: Emerging role as a dominant electricity generation technology in the 21st century," *in International Conference on Microelectronics, 2012, pp. 53{63. 6.*

[2] "Trends in Photovoltaic application, survey report of selected IEA countries between 1992 and 2002," *International Energy Agency Photovoltaic Power system, IEA, PVPS T1-12:2003, 2003,*

[3] Prajna Paramita Dash, Student Member, IEEE, and Mehrdad Kazerani, Senior Member, IEEE "Dynamic Modeling and Performance Analysis of a Grid-Connected Current-Source Inverter-Based Photovoltaic System" *IEEE Transaction on sustainable energy, vol2, no.4 , October 2011*

[4] E. Koutroulis and F. Blaabjerg, "Methods for the optimal design of grid-connected PV inverters," *International Journal of Renewable Energy Research, vol. 1, no. 2,pp. 54{64, 2011. 8*

[5] H. Kim and K. Kim,"Filter design for grid-connected PV inverters," in International conference on Sustaianble Energy Technologies, 2008, pp. 1070

[6] National electric code," *National Fire Protection Association Inc., 2002. 9*

[7] Saurabh Singh Kashyap and Dr. K.S.Verma "Grid Connected Photovoltaic System, An Assessment of Performance" *NPESC-14_110 April 2014*